Open access • Journal Article • DOI:10.1122/1.3193720

Structural analysis of non-aqueous layered silicate suspensions subjected to shear flow — Source link

Christophe Mobuchon, Pierre J. Carreau, Marie-Claude Heuzey

Published on: 10 Sep 2009 - Journal of Rheology (The Society of Rheology)

Topics: Rheometry, Characteristic length, Rheology and Silicate

Structural analysis of non-aqueous layered silicate suspensions subjected to shear flow

Christophe Mobuchon, Marie-Claude Heuzey, Pierre J. Carreau

Structural analysis of non-aqueous layered silicate suspensions subjected to shear flow

Christophe Mobuchon, Pierre J. Carreau,[a] and Marie-Claude Heuzey

Department of Chemical Engineering, Center for Applied Research on Polymers and Composites (CREPEC), Ecole Polytechnique, P.O. Box 6079, Stn. Centre-Ville, Montreal, Quebec H3C3A7, Canada

Non-aqueous layered silicate suspensions exhibit a complex rheological behavior due to a multiple length scale structure, which is sensitive to flow and flow history. In the present work, the nature of flow-induced non-equilibrium and metastable structures in non-aqueous layered silicate suspensions based on natural and organo-modified sodium montmorillonites was examined using rheometry and confocal laser scanning microscopy (CLSM). The scaling behavior of their linear and non-linear viscoelastic properties was investigated. Based on fractal scaling theories, the scaling laws of the solid-like properties were ascribed to the presence of space-filling percolating networks consisting of clusters with a mass-fractal dimensionality, $D_f \sim 2$. CLSM allowed us to detect the formation of aggregates under flow and to characterize their microscopic length scale. The shear-rate dependency of the microstructure characteristic length scale was attributed to a reversible shear-induced aggregation process. Upon cessation of flow, the observed thixotropic behavior of these suspensions was inferred from the CLSM observations to stem from local rearrangements at the nano-scale.

I. INTRODUCTION

Colloids and nanoparticles have found increasing uses as rheological modifiers in paints, inks, lubricating greases, cosmetics, and pharmaceutical formulations. More recently, layered silicates of the smectite group have attracted great interests as nanoscale fillers for reinforcement of polymers [polymer nanocomposites (PNCs)] [Patel *et al.* (2006)]. Due to their particular nature, suspensions based on colloids and nanoparticles are quite complex since they undergo a fluid-to-solid transition with the formation of disordered solids defined by their dynamics and elasticity [Trappe and Sandkuhler (2004)].

For attractive colloidal particles, Trappe *et al.* (2001) recently proposed a phase diagram that is a function of the particle volume fraction, energy of interparticle attraction, and applied stress. The non-equilibrium solid states of this diagram include two extremes: hard sphere colloidal glasses at high volume fraction, ϕ, and low attractive potential, U, and strongly attractive colloidal gels at low ϕ and high U. For the limiting case of hard-sphere colloidal particles (for which the interaction potential between spherical par-

[a]Author to whom correspondence should be addressed; electronic mail: pierre.carreau@polymtl.ca

ticles is determined solely by the excluded volume), the suspensions undergo a liquid-to-glass transition at a volume fraction $\phi_g \sim 0.58$ due to the crowding of single particles. The solid-like properties of colloidal glasses stem from the permanent kinetic trapping of the particles within cages formed by their nearest neighbors [Trappe and Sandkuhler (2004)]. The resistance to configuration changes of these cages provides a mechanism for energy storage (and viscous dissipation), which gives rise to a low-frequency plateau storage modulus [Crassous *et al.* (2005); Helgeson *et al.* (2007); Mason and Weitz (1995)]. Models based on the mode coupling theory predict a low-frequency plateau storage modulus [Mason and Weitz (1995)], G_0', scaling with the volume fraction, ϕ, as $G_0'(\phi) \ \alpha(\phi)^n$ with $n \approx 0.3-0.5$ [Götze (1991); Zaccarelli *et al.* (2001)].

On the other hand, at low volume fractions, attractive spherical particles aggregate as they form self-similar clusters with a mass, M, scaling with their average size, ξ_c, as $M(\xi_c) \alpha M_0(\xi_c / a_{eff})^{D_f}$, where D_f is the mass-fractal dimensionality, a_{eff} is a characteristic size, and M_0 is the mass of the cluster compact building blocks. Aggregation of clusters ultimately leads to a space-filling percolating network exhibiting macroscopic non-ergodicity (i.e., breakdown in the equivalence of time and space averages) and, therefore, to a sol-to-gel transition. The solid-like behavior of colloidal gels originates from the stress bearing network made of close packed clusters. The dependency of the network elasticity on the volume fraction ϕ was shown to be stronger than predicted for colloidal glasses, with $G_0'(\phi) \ \alpha(\phi)^n$ and $n \approx 4$ (spherical colloidal particles) [Buscall *et al.* (1988); Khan and Zoeller (1993); Piau *et al.* (1999); Saint-Michel *et al.* (2003); Shih *et al.* (1990); Yziquel *et al.* (1999)]. Scaling models linking the fractal microscopic structure parameters to the macroscopic elastic properties of gels are presented in detail in the next section. Despite the structural differences between colloidal glasses and gels, their solid-like properties are similar in nature. Both result from the physical jamming or crowding of the characteristic particles within the suspensions: single particles in the case of glasses and clusters in the case of gels [Segrè *et al.* (2001)].

Between the two limiting cases of glasses and gels, the structure and elasticity of colloidal suspensions in non-equilibrium solid states remain to be investigated. If suspensions of spherical colloidal particles have attracted a large amount of interest, attractive colloidal suspensions of anisotropic particles have been the subject of fewer investigations. The liquid-to-glass transition of suspensions containing anisotropic colloidal particles is expected to occur at volume fraction much lower than their maximum packing fraction since the excluded volume of anisotropic particles is larger than their actual volume [Jogun and Zukoski (1996, 1999)]. The particle anisotropy may also lead to differences associated with their orientation and consequently to a more complex picture of the non-equilibrium solid states [Lyatskaya and Balazs (1998)].

Layered silicate particles are highly anisotropic. The most commonly used layered silicate is montmorillonite, in which the individual layers are about 1.2 nm thick, 320–400 nm long, and 250 nm wide for the larger ones [Cadene *et al.* (2005)]. Aqueous layered silicate suspensions undergo phase transitions controlled by repulsive or attractive interactions dependent on ionic strength and *p*H. The establishment of their state diagram has gradually emerged in recent years [Kroon *et al.* (1998); Michot *et al.* (2004); Mourchid *et al.* (1995); Pignon *et al.* (1996, 1997a, 1997b, 1998); Ruzicka *et al.* (2006); Shalkevich *et al.* (2007); Tanaka *et al.* (2004, 2005); Tombacz and Szekeres (2004)]. With increasing ionic strength, clay layers become attractive and the state diagram is expected to gradually follow the jamming phase diagram for attractive particles proposed by Trappe and Sandkuhler (2004). In the same way, non-aqueous layered silicate suspensions belong to attractive colloidal suspensions as the repulsive electrostatic interactions are negligible and, therefore, should exhibit non-equilibrium fluid-to-solid transitions of

the jamming phase diagram. Note that due to the high aspect ratio of the clay layers, the liquid-to-glass transition is not restricted to high volume fractions and is expected at low volume fractions where gelation can occur [see developments of King *et al.* (2007) and Ren *et al.* (2000) for the calculation of ϕ_g]. Actually, a fluid-to-solid transition has been observed for polymer layered silicate nanocomposites with the development of a low-frequency plateau storage modulus increasing with volume fraction [see for instances Aubry *et al.* (2005), Lim and Park (2001), and Ren *et al.* (2000)]. The non-terminal flow behavior is usually attributed to the formation of a percolated three-dimensional network of clay layers or tactoids and, thus, to a fluid-to-glass transition [Galgali *et al.* (2001); Mitchell and Krishnamoorti (2002); Ren *et al.* (2000)]. A sol-to-gel transition through the formation of fractal networks has been lately considered [Durmus *et al.* (2007); Vermant *et al.* (2007)]. Until now, the literature reveals a lack of studies of colloidal attractive suspensions in light of jamming phase diagrams including structural and rheological descriptions of their non-equilibrium states.

In the current paper, we investigate the nature of the non-equilibrium and metastable solid states of polar and non-polar non-aqueous layered silicate suspensions. At first, their viscoelastic properties are reported and their scaling behavior is explored according to both the volume fraction and the temperature (interaction energy). Afterwards, the rheological scaling laws observed are correlated with the clay microstructure. Confocal laser scanning microscopy (CLSM) is also used to verify the existence of a space-filling network and the observed length scales are compared to the predictions of fractal scaling theories. Finally, the flow history dependency of layered silicate suspensions reported in a previous publication [Mobuchon *et al.* (2007)] is explained by the investigation of the network evolution under flow and at rest.

II. THEORETICAL BACKGROUND

Fractal scaling theories

In the framework of fractal scaling theories [Bremer *et al.* (1989); Buscall *et al.* (1988); Shih *et al.* (1990); Wu and Morbidelli (2001)], the network structure is considered to result from the close packing of mass-fractal clusters with an average size ξ_c following a scaling relation with the volume fraction ϕ [Mellema *et al.* (2000)]

$$\xi_c = a_{eff}\phi^{1/(D_f-d)}, \quad 1 \leq D_f \leq 3, \tag{1}$$

where d is the Euclidian dimension of the system and a_{eff} is the characteristic size of the cluster compact building blocks. The cluster mass-fractal dimensionality, D_f, can be interpreted as a measure of the compactness of the clusters and depends on the mechanism of particle aggregation. A value of 3 for D_f corresponds to uniform dense (non-fractal) clusters, while diffusion-limited aggregation and reaction-limited cluster aggregation lead to values of 1.8 and 2.1, respectively [Bushell *et al.* (2002)]. As self-similarity is restricted to length scales below ξ_c, two levels of structure can be distinguished: fractal intra-microstructure of the clusters and inter-microstructure characterized by the cluster interactions.

Recently, Wu and Morbidelli (2001) developed a scaling model, based on the work of Shih *et al.* (1990), to relate the microscopic structural parameters to the macroscopic elastic properties. In their model, the intra- and inter-microscopic contributions to elasticity are considered in series to give the overall microscopic elasticity, K_{eff},

$$1/K_{eff} = 1/K_{\xi_c} + 1/K_l, \tag{2}$$

where K_{ξ_c} and K_l are the intra- and inter-microscopic elastic constants, respectively. According to Shih *et al.* (1990), the elastic properties of a cluster are dominated by its backbone, which is approximated as a linear chain of springs with a fractal dimension, $1 < x < D_f$, different from that of the cluster. The intra-microscopic elastic constant K_{ξ_c} can then be related to ξ_c using the following Khantor-Webman relation [Kantor and Webman (1984); Krall and Weitz (1998)]:

$$K_{\xi_c} = K_0(a_{eff}/\xi_c)^{2+x}, \tag{3}$$

where K_0 is the spring constant of a bond between two cluster compact building blocks. On the other hand, the inter-microscopic elastic constant, K_l, refers to the interactions between the clusters and, therefore, is independent of the intra-microscopic structural parameters. The macroscopic elastic modulus, G', can be related to K_{eff} as

$$G' = \frac{K_{eff}}{\xi_c} = \frac{1}{\xi_c}\frac{K_{\xi_c}}{1 + (K_{\xi_c}/K_l)} \cong \frac{1}{\xi_c}K_{\xi_c}\left(\frac{K_l}{K_{\xi_c}}\right)^{\alpha}, \tag{4}$$

where α is a constant in the range of [0, 1], which depends on the given range of K_{ξ_c}/K_l. The dependence of G' on ϕ is then derived from Eq. (5),

$$G' \cong \frac{K}{a_{eff}}\phi^{n=\beta/d-D_f} \quad \text{with} \quad \beta = (d-2) + (2+x)(1-\alpha) \quad \text{and} \quad K = K_l^{\alpha}K_0^{1-\alpha}. \tag{5}$$

This scaling model was also extended for the strain limit of linearity, γ^0, following the original approach of Shih *et al.* (1990),

$$\gamma^0 \propto \phi^B \quad \text{with} \quad B = (d-\beta-1)/(d-D_f). \tag{6}$$

In the case of the strong-link regime, where links between the neighboring clusters are stronger than the intra-microscopic links within the clusters, $\alpha = 0$ and Eq. (6) predicts that the limit of linearity decreases with increasing ϕ. In contrast, γ^0 increases with increasing ϕ for the limiting condition of weak-link regime ($\alpha = 1$) for which the breaking of the network occurs at the intercluster links. Finally, the two preceding scaling laws [Eqs. (5) and (6)] lead to the following scaling law for the yield stress, σ_0:

$$\sigma_0 = G'\gamma^0 \propto \phi^{t=(d-1)/(d-D_f)}. \tag{7}$$

III. MATERIALS AND METHODS

A. Materials and preparation methods

1. Polar suspensions

The polar system used in this study consists of a natural layered silicate, a sodium montmorillonite, $M_x[Al_{2-y}Mg_y]Si_4O_{10}[OH]_2 \cdot nH_2O$, (Cloisite Na^+, Southern Clay products, $\rho = 2.86$ g/mL), dispersed in a Newtonian polyalkylene glycol, $HO[C_2H_4O]_x[C_3H_6O]_y-[C_2H_4O]_xH$, (Plurasafe WT 90000, BASF) of molar mass around 1500 g/mol, viscosity of 59 Pa s and density of 1.09 g/mL at 25 °C. Clay volume fractions used are comprised between 0.001 and 0.005. The colloidal individual montmorillonite layers can be described as elliptical platelets 1.2 nm thick with lateral dimensions of 0.25–0.4 μm [Cadene *et al.* (2005)]. The clay was added to the polyalkylene glycol via solution mixing as follows. First, natural clay platelets were exfoliated in de-ionized water using an ultrasound probe (Sonics & Material) [Ho *et al.* (2001)]. The

*p*H was adjusted to approximately 9.5 in order to avoid dissolution of the silicate [Thompson and Butterworth (1992)]. Polyalkylene glycol was then added to the aqueous clay suspension and the entire mixture exposed to ultrasonication before extraction of the de-ionized water in a high vacuum oven at 40 °C. For the clay volume fractions used, the resulting suspensions were homogeneous translucid gels, stable over several months. Other methods aiming at directly incorporating the nanoclay in polyalkylene glycol, based on both sonication and high shear mixing, were observed not to induce gel formation. The mechanical energy involved in these two methods, conjugated with the good affinity between the clay and the polyalkylene glycol, does not suffice to overcome the energy of adhesion between the clay layers and hence hinders the polyalkylene glycol intercalation [Bousmina (2006)].

For the confocal laser scanning microscopic studies described below, the natural clay was tagged with Safranine-O, $C_{20}H_{19}ClN_4$, (Sigma-Aldrich), a fluorescent cationic dye, taking advantage of its cation exchange capacity (CEC). Fluorescent suspensions were prepared using the same procedure described above with the addition of an appropriate amount of Safranine-O [equivalent to 5% of the clay CEC (92.6 mmol/100 g clay)] in de-ionized water. The low amount of adsorbed Safranine-O on the clay surface is later shown not to affect noticeably the rheological properties of the suspensions.

2. Non-polar suspensions

The non-polar system is based on a sodium montmorillonite (Cloisite® 15A, Southern Clay products) organically modified with a dimethyl dihydrogenated quaternary ammonium salt, $CH_3CH_3N^+HTHT$, where HT refers to the hydrogenated tallow of various carbon chain lengths: C_{18} (65%), C_{16} (30%), and C_{14} (5%). The longest C_{18} chains have an estimated length of 2.67 nm [Ho *et al.* (2001)]. A second organomodified montmorillonite (Cloisite® 30B, Southern Clay products) with a methyl dihydroxyethyl, quaternary ammonium salt, $CH_3N^+[CH_2OH]_2$, was also used for comparison. The non-polar suspending fluid was a mixture of two Newtonian polybutenes, $R[CH_2CCH_3CH_3]_x[CH_2]_yR$, of different molar mass, respectively, 910 g/mol (76.4 mass %, Indopol H100, BP) and 1300 g/mol (23.6 mass %, Indopol H300, BP) with an overall viscosity of 28.5 Pa s and a density of 0.89 g/mL at 25 °C. Clay volume fractions used were comprised between 0.0075 and 0.040. The non-polar suspensions were prepared following two different procedures, both resulting in stable homogeneous translucid gels. The first procedure consisted of incorporating directly the organomodified montmorillonite by ultrasonication. Details about the procedure and characterization of the corresponding dispersions are reported elsewhere [Mobuchon *et al.* (2007)]. The second procedure via solution mixing from toluene is equivalent to the procedure described before for the polar suspension. Toluene was selected, since the organomodified montmorillonite can be dispersed in it to yield a transparent gel [Ho *et al.* (2001)]. The fluorescent organoclay used for the CLSM studies was prepared separately from its suspensions. Safranine-O was dissolved in ethanol/de-ionized water (1:1) solution and stirred overnight after the addition of organoclay. The treated organoclay was filtered and washed with a hot solution of ethanol in de-ionized water (1:1 at first and then 4:1) until the filtrate became colorless. The fluorescent organoclay was then dried in a vacuum oven overnight and pulverized into fine powder. The non-polar suspensions based on the resulting fluorescent organoclay were prepared via the previously described ultrasonication and solution mixing methods.

B. Rheometry

The rheological characterization of the suspensions was performed using a stress-controlled rheometer (Anton-Paar, Physica MCR 501). A cone-and-plate geometry with a radius of 50 mm and a cone angle of 0.04 rad was used for the tests performed at 25 °C, while a parallel plate geometry of 50 mm radius was employed for the investigation of the temperature effect. Actually, the true gap option of the MCR parallel plate geometry allows to monitor the gap and to keep it constant while the temperature of the instrument is changing. The steady-shear viscosity was measured by applying stepwise shear rate-decreasing ramps from 25 to 10^{-3} s^{-1}. Linear viscoelastic measurements were conducted at a fixed strain of 0.005, which is below the limits of linearity, γ^0, for all suspensions. The limits of linearity were determined, at a frequency of 6.28 rad s^{-1}, as the strain at which G' deviates from its plateau value by 10%. To ensure controlled initial microstructures [Mobuchon *et al.* (2007)], all the dynamic measurements were preceded by a pre-shearing at a defined shear rate $\dot{\gamma}_i$ until steady state was reached and then followed by a rest time of 5400 s. For the stepwise shear rate measurements, data were considered after a period of 0.04 s, time required to reach the specified shear rate within an error of less than 2%. The standard deviation on the rheological data was estimated to be less than $\pm 9\%$. Investigations using various gaps and different roughness values for the parallel plates ruled out slip or wall effects for the two types of suspensions. However, flow instabilities with sample fracture localized in the middle of the gap were observed for clay volume fractions above 0.005 and 0.03 for the polar and non-polar suspensions, respectively, prepared by solution mixing (this phenomenon was never observed for the non-polar suspensions prepared by ultrasonication). The fracture was observed independently of the gap used and for the entire shear rate range investigated (from 25 to 10^{-3} s^{-1}). At low shear rates, the occurrence of fracture was inferred from the measured stresses, which were smaller than the value for the suspending fluid alone. The identification of the mechanisms leading to sample fracture is beyond the scope of this paper, but one may argue that the high elasticity of these suspensions drives this phenomenon. Hence, all results reported here for samples prepared by solution mixing are for volume fractions smaller than the critical values for sample fracture. For all the dynamic data reported in this paper, the standard deviation was estimated to be within $\pm 5\%$.

C. Optical measurements

CLSM

The micro-scale structures of the clay suspensions were directly observed using a confocal laser scanning microscope (Zeiss, Axioplan 2 & LSM 510 META) equipped with a commercial optical shear cell (Linkam Scientific Instruments, CSS450). The homogeneity of the imposed shear flow through the gap was established with a long working distance lens (Leica, $20\times/0.33$ numerical aperture, NA). A higher resolution oil immersion $40\times/1.3$ NA lens of 0.2 mm working distance (Carl-Zeiss, Plan-Neofluar) and a water immersion $40\times/1.2$ NA lens of 0.29 mm working distance (Carl-Zeiss, C-Apochromat) were used to observe the suspension microstructures. The original top plate of the shear cell is not compatible with a low working distance lens due to the thickness of its fixed parallel quartz disk. It was therefore necessary to replace it by a homemade lid with a glass cover of 160 μm depth that acted as the fixed parallel plate. The Safranine-O was excited at 488 nm and its fluorescence was detected at wavelengths λ above 560 nm through a filter system. The lateral and focal plane resolutions were estimated to be about 0.17 ($\approx 0.4\lambda/\mathrm{NA}$) and 0.46($\approx 1.4\lambda/\mathrm{n.a.}^2$)$\mu$m [Pawley (2006)], respectively. The spatial resolution of the images was chosen above the lateral resolution

of the CLSM and the dynamic range of their intensity was 8 bits. The time resolution of the CLSM turned out to be enough to acquire images under flow at shear rates up to 0.1 s^{-1} and during relaxation. The real-space images were quantitatively analyzed to extract their characteristic length scale and to assess their isotropy [Kaufman *et al.* (2005); Lin *et al.* (2007)]. The image processing consisted first in a binarization of gray scale images with the threshold defined by their mean intensity and pixels with intensity above the threshold were considered to be part of the clay particles. A two-dimensional median filtering using two-by-two neighborhoods was then applied to remove "salt and pepper" noise (isolated pixels). The distances, ξ, between nearest neighbors of pixels above the threshold were then determined within each row (x) and column (y). Their distribution, $P(\xi)$, along these directions follows an exponential decay: $P(\xi) \propto \exp\{-2\xi/\xi_0\}$, where ξ_0 represents an average measure of the spatial correlation at the micro-scale. The same row and column distributions, $P(\xi)$, and density distribution are expected in the case of an isotropic image. Finally, the ratio of the number of pixels above the threshold with the total number of pixels was used to estimate the amount, A, of surface occupied by the clay particles.

IV. RESULTS AND DISCUSSION

A. Flow induced non-equilibrium and metastable structures

In non-aqueous systems, the interaction potential between clay platelets includes short-range van der Waals attraction and forces induced by polymer chains and excluded volume. The potential of the van der Waals forces can be quantified by the Hamaker constant A_H, which is a function of temperature and differences in refractive index and dielectric constants of the two phases. In the case of the non-polar suspensions, a steric barrier to the van der Waals forces is expected due to the compatibility between the surfactant hydrocarbon tails and the suspending fluid. A steric barrier is also expected in polar suspensions with the adsorption, during the solution mixing step, of the polyalkylene glycol chains on the clay surface. Depending on the extent of steric stabilization, the suspensions can belong to hard solid dispersions, where the van der Waals interactions are negligible relative to the Brownian motion and in other cases, to the weakly or strongly aggregated dispersions. Nevertheless, it will be shown later that the behavior and structure of both types of suspensions are fairly similar in nature, but for on a quite different range of clay concentration.

As previously reported [Mobuchon *et al.* (2007)], the linear viscoelastic properties of layered silicate suspensions are strongly correlated with the flow history. This behavior is illustrated in Fig. 1(a) for the non-polar suspension prepared by ultrasonication for $\phi = 0.01$ and in Fig. 1(b) for the polar suspension for $\phi = 0.003$ ($\omega = 126.5$ rad s^{-1}). Upon cessation of the steady-shear flow, the storage modulus, G', is shown to grow from an initial value G'_i to a time invariant value G'_∞ following an exponential form adapted by Mobuchon *et al.* (2007) from Dullaert and Mewis (2005)

$$G'(t) = G'_i + (G'_\infty - G'_i)\left(1 - \exp\left[-\left(\frac{t}{\tau}\right)^m\right]\right), \tag{8}$$

with m the stretching exponent and τ the characteristic time. The values of G'_i and G'_∞ resulting from the non-polar suspension data of Fig. 1(a) are shown in Fig. 2(a) (unfilled and filled circles, respectively) to significantly decrease from high to low plateau values for increasing pre-shearing rate, $\dot{\gamma}_i$. Therefore the non-equilibrium structures under flow, characterized by G'_i, evolve at rest toward different metastable structures with larger elastic modulus G'_∞ values. In a similar fashion, the linear viscoelastic properties of the

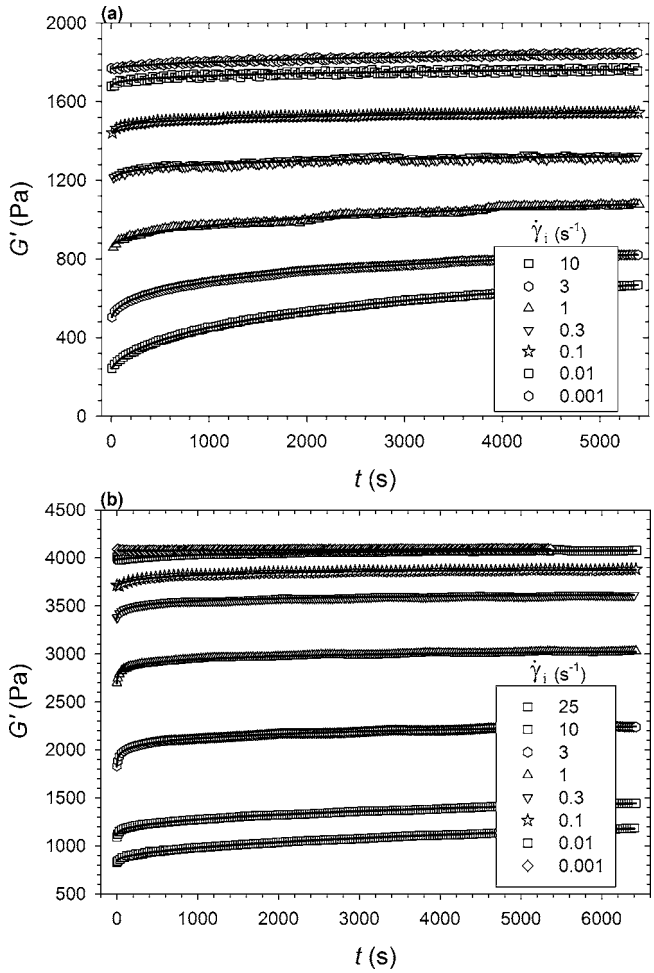

FIG. 1. G' as a function of time measured at a frequency of 125.6 rad s^{-1} upon cessation of steady shear flow. T=25 °C. Symbols indicate the values of the initial pre-shear rate $\dot{\gamma}_i$; solid lines represent best fits using Eq. (8). (a) The non-polar suspension prepared by ultrasonication for ϕ=0.01 and (b) the polar suspension for ϕ =0.003.

polar suspension [Fig. 2(b)] are sensitive to the flow history, but differ in the extent of the structural recovery that tends to vanish as the pre-shearing amplitude decreases. It is noteworthy to mention that a similar flow history dependency was also observed for organo modified suspensions at higher volume fraction (0.04, [Mobuchon *et al.* (2007)]) and higher temperature (40 °C, results not shown) and prepared by ultrasonication with synthetic layer silicates of different aspect ratios, p, (results not shown): a hectorite with $p \approx 50$ (Lucentite SANS, CBC Co.) and a fluoromica with $p \leq 6000$ (Somasif MAE, CBC Co.). This behavior appears to be a universal feature of strongly attractive colloidal suspensions.

As a consequence of the flow history dependency, the polar and non-polar suspensions undergo a fluid-to-solid-like transition due to pre-shearing. The transition is depicted in Fig. 3 for the polar suspension (ϕ=0.003) where its storage modulus as a function of frequency is reported after different initial pre-shear rates $\dot{\gamma}_i$. The low frequency elastic

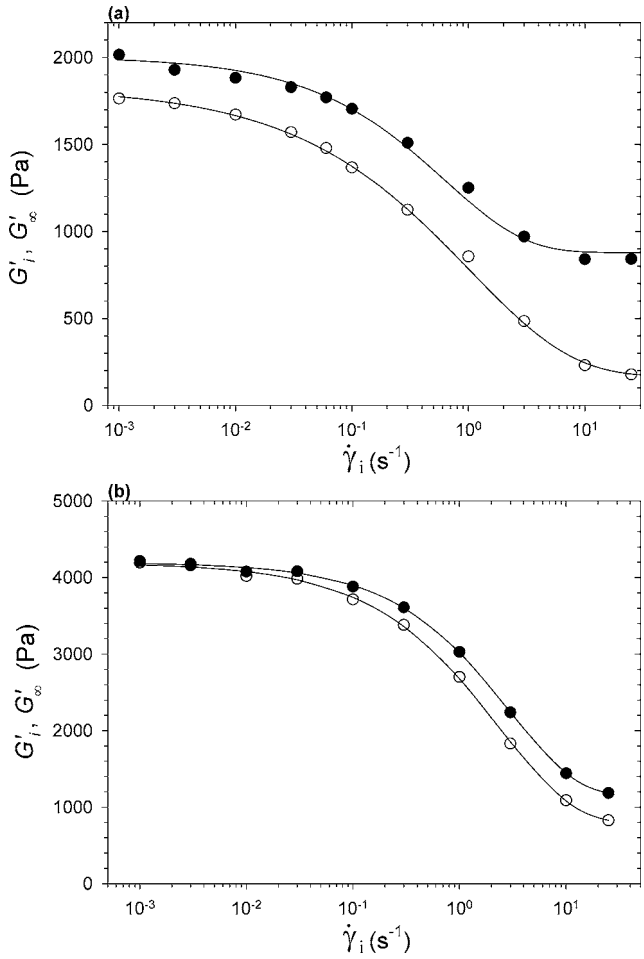

FIG. 2. Dependences of G'_i (unfilled symbols) and G'_∞ (filled symbols) on the pre-shearing amplitude. (a) Non-polar suspension prepared by ultrasonication for ϕ=0.01; (b) polar suspension prepared by solution mixing with ϕ=0.003. All measurements were done at 126.5 rad s^{-1}. T=25 °C. Solid lines are drawn to guide the eyes.

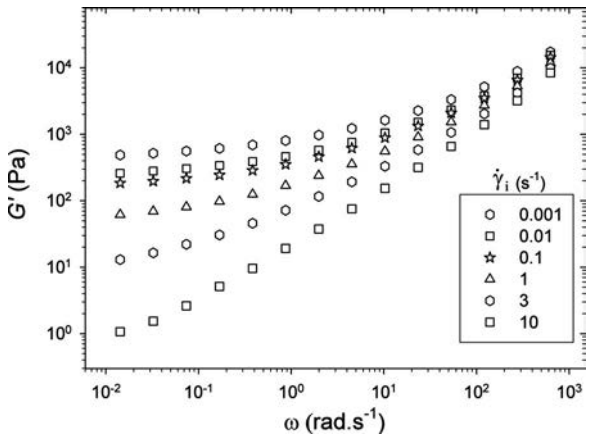

FIG. 3. G' as a function of ω of the polar suspension (ϕ=0.003) for different pre-shear rates. T=25 °C.

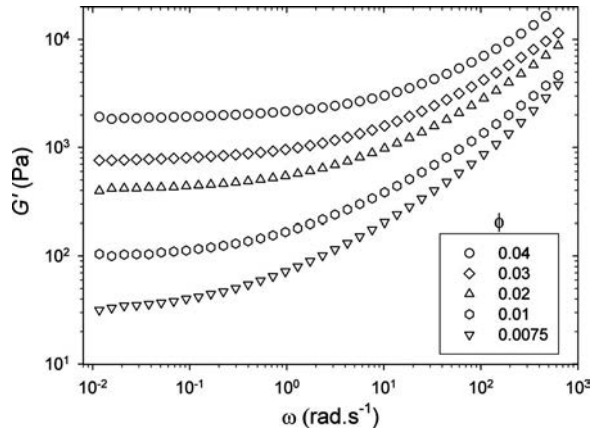

FIG. 4. G' as a function of ω of the non-polar suspensions prepared by ultrasonication for different volume fractions ϕ. The suspensions were pre-sheared at a $\dot{\gamma}_i = 10^{-3}$ s^{-1} and then allowed to rest during 5400 s. T =25 °C.

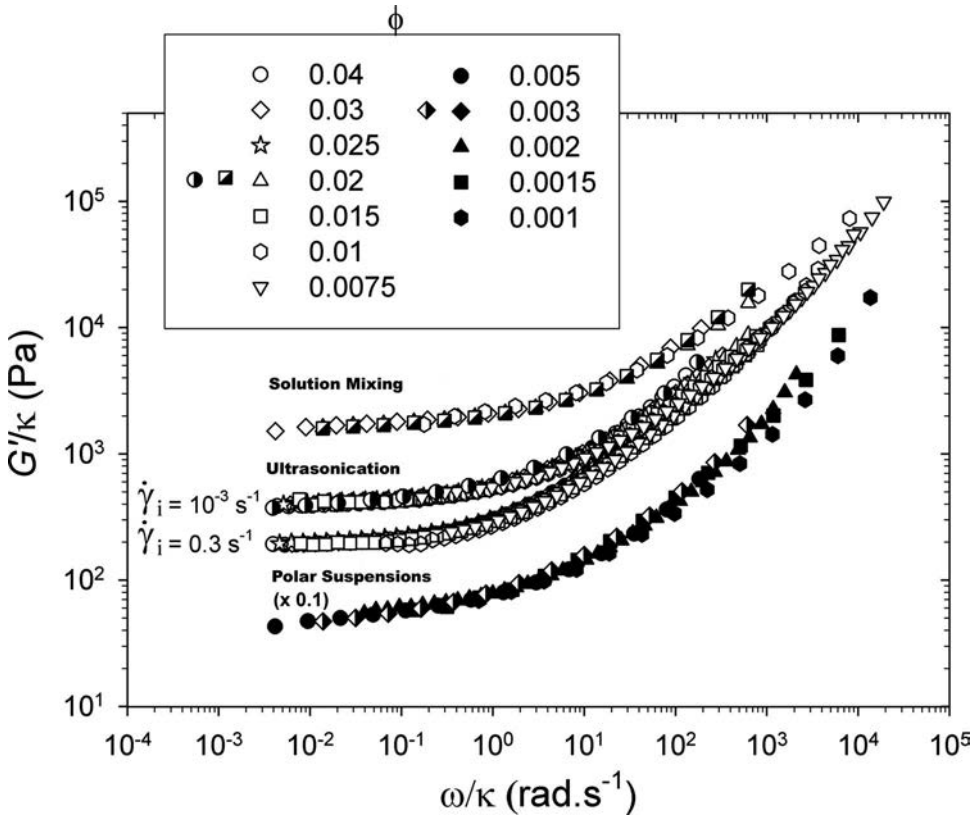

FIG. 5. Scaling behavior of G' as a function of scaled frequency ω/κ as ϕ is varied for the polar suspensions (ϕ_{ref}=0.003) and the two non-polar suspensions prepared by solution mixing and ultrasonication (ϕ_{ref} =0.020). The fluorescent suspensions (with Safranine-○) are indicated with the following symbols: [◑] the non-polar suspension prepared by ultrasonication with ϕ=0.020; [◪] the non-polar suspension prepared by solution mixing for ϕ=0.02; [⬗] the polar suspension for ϕ=0.003.

modulus measured after a 5400 s rest time is actually shown to evolve from a liquid-like behavior for high pre-shearing rates toward a non-terminal flow behavior (i.e., nearly independent of ω) as the initial pre-shear rate is decreased.

B. Scaling behavior with volume fraction

Figure 4 shows the frequency dependence of the elastic modulus at various volume fractions, ϕ, ranging from 0.0075 to 0.040 for the non-polar suspensions prepared by ultrasonication. Prior to all measurements, the samples were systematically pre-sheared at a low pre-shearing rate ($\dot{\gamma}_i = 10^{-3}$ s^{-1}) and then allowed to rest during 5400 s to ensure similar flow history. As the volume fraction increases, the elastic modulus becomes significantly larger and displays a wider plateau at low frequencies, characterized by G_0'. The dependence of the plateau value, G_0', on ϕ will be discussed further in relation to the nature of the clay network. An excellent superposition of the linear viscoelastic properties with the volume fraction is obtained based on the scaling factor κ as shown in Fig. 5. κ is defined as the ratio of G_0' and a reference modulus, G_{0r}', corresponding to a volume fraction, ϕ_{ref}, arbitrarily chosen to be 0.020. This scaling is similar to that reported by Hobbie and Fry (2007) for concentrated nanotube suspensions. It is also in agreement with the universal scaling behavior of weakly attractive particles discussed by Trappe and Weitz (2000; 2001). Figure 5 shows that the scaling behavior applies for all data obtained under various pre-shearing rates, preparation methods, and different suspensions. Rather

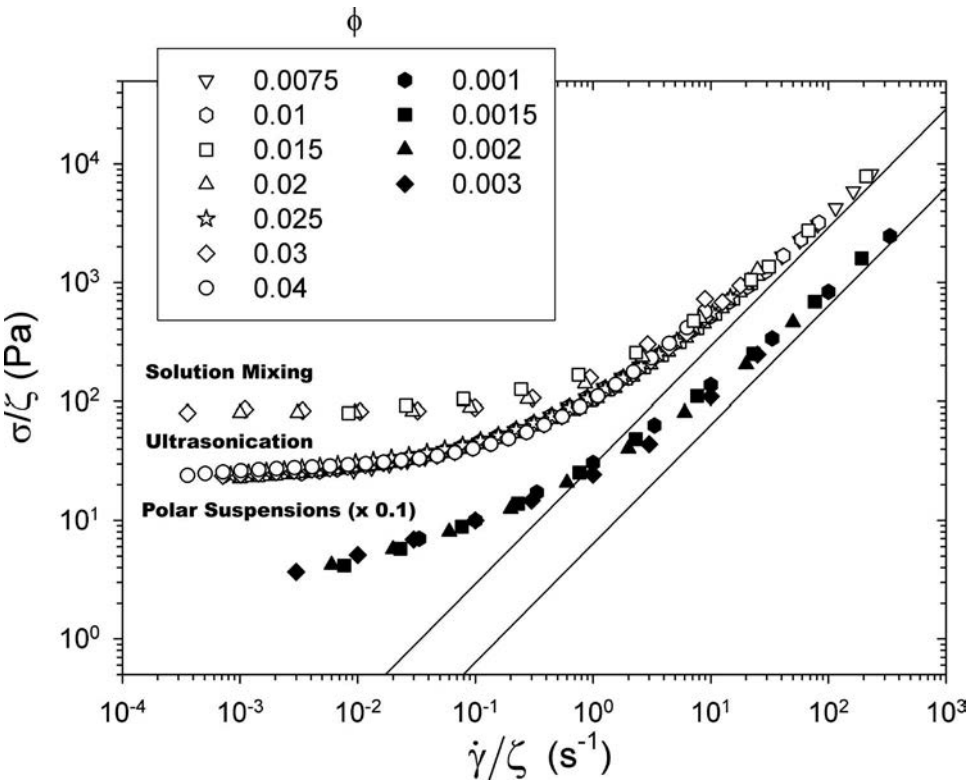

FIG. 6. Scaling behavior of σ as a function of scaled shear rate $\dot{\gamma}/\xi$ as ϕ is varied for the polar suspensions (ϕ_{ref}=0.003; filled symbols) and the two non-polar suspensions (unfilled symbols) prepared by solution mixing and ultrasonication (ϕ_{ref}=0.020). Solid lines represent the shear stress vs shear rate of the suspending fluids.

surprisingly, the reduced storage modulus of the polar suspensions shows a similar behavior than that of the non-polar suspensions, while the reference volume fraction is nearly ten times smaller (ϕ_{ref}=0.003). Note that for the fluorescent suspensions used in CLSM, the low-frequency data of G' are unaffected by the presence of Safranine-O (semi-filled symbols in Fig. 5), suggesting that it does not perturb the interaction potential between the clay platelets.

Similarly, a scaling is proposed for the steady-state data (stress vs. shear rate), suggested by the Bingham equation and based on the apparent yield stress. Actually, the behavior of the layered silicate suspensions is typical of a yield stress material, as described by the Bingham equation: $\sigma=\sigma_0+\mu_0\dot{\gamma}$, where σ, σ_0, and μ_0 are the steady stress, the apparent yield stress, and the high-shear rate viscosity of the suspension, respectively. The shift factor, $\xi=\sigma_0/\sigma_{0|\phi_{ref}}$, where $\sigma_{0|\phi_{ref}}$ is the apparent yield stress for the reference volume fraction, is applied to reduce the steady stress σ and the shear rate $\dot{\gamma}$. Figure 6 shows that the scaling effectively reduces the data of the non-polar suspensions prepared

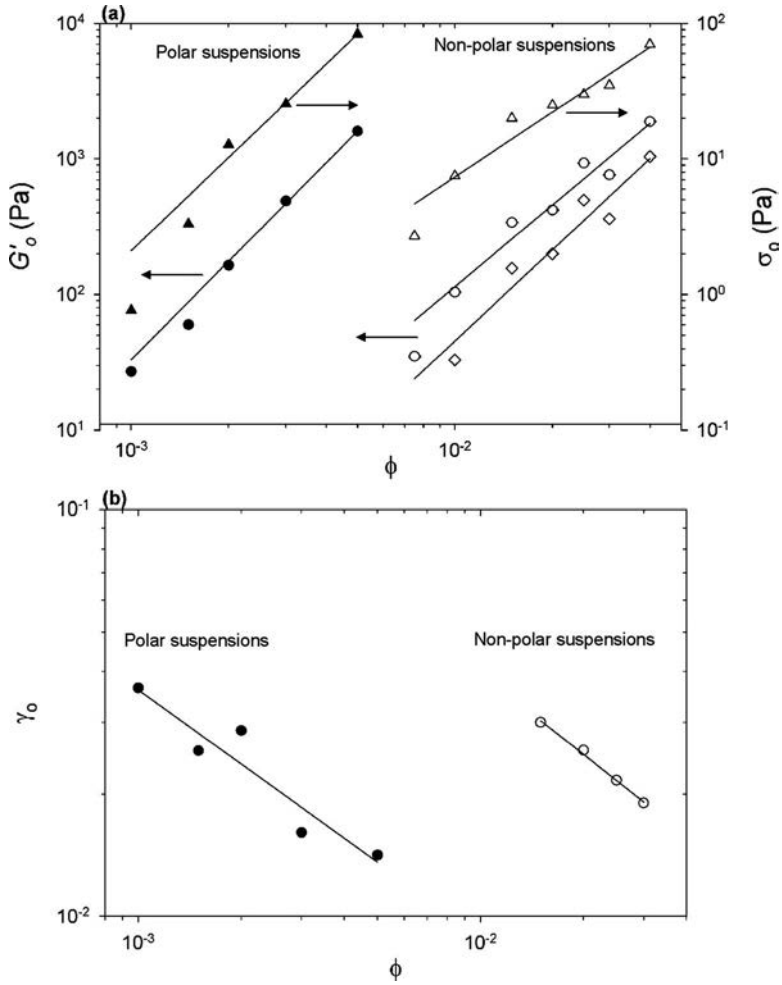

FIG. 7. (a) Variations of G'_0 (circles: $\dot{\gamma}_i=10^{-3}$ s^{-1} and diamonds: $\dot{\gamma}_i=0.3$ s^{-1}) and of σ_0 (triangles) as functions of the volume fraction ϕ; (b) variation of γ^0 with ϕ for the non-polar suspensions prepared by ultrasonication (unfilled symbols) and the polar dispersion (filled symbols).

by ultrasonication and by solution mixing in single master curves (ϕ_{ref}=0.020). On the other hand, the yield stress for the polar suspensions was not well defined and it was deduced from the scaling procedure itself. A similar scaling behavior was observed for concentrated nanotube suspensions by Hobbie and Fry (2007) and is expected for other Bingham fluids [Trappe and Weitz (2000)]. The values of the plateau (low frequency) storage modulus G'_0 and of the yield stresses σ_0 used to calculate the shift factors, κ and ξ, are plotted in Fig. 7(a) as functions of the clay volume fraction, while Fig. 7(b) presents the limit of linearity γ^0 of the two suspensions. The similarity within the behavior of these suspensions is discussed in the scope of the microstructure in Sec. IV.

C. Scaling behavior with temperature

The significant effect of temperature, T, on the non-equilibrium structures of the non-polar suspension prepared by ultrasonication (ϕ=0.040) and the polar suspension (ϕ=0.003) is illustrated in Fig. 8. The stress, σ, reduced by the contribution of the suspending fluid, σ_m, is plotted at different temperatures as a function of the hydrodynamic stress, $\dot{\gamma}\eta$, where η is the viscosity of the suspension at high shear rate. Since the suspending fluids are Newtonian, the reduced stresses correspond to the contributions of the clay structures. The hydrodynamic contributions vary considerably over the temperature range covered experimentally. This is principally due to the viscosity changes of the suspending fluids with temperature (multiplied by ~8 and ~5 for the non-polar and polar suspensions, respectively, when the temperature is decreased from 65 to 15 °C). The non-superposition of the reduced stresses brings out the strong temperature dependency of the interaction potential between the clay platelets. In the same manner as that for the volume fraction, the shift factor ξ based on yield stress allows to superpose the flow curves at different temperatures (filled symbols in Fig. 8 with T_{ref}=40 and 65 °C for the non-polar and polar suspensions, respectively). It will be shown below that, remarkably, the shift factors ξ of the non-polar and polar suspensions follow the same exponential decay dependency with temperature.

To investigate the effect of temperature on the metastable structures, the frequency dependency of the elastic modulus was measured in the same temperature range as the

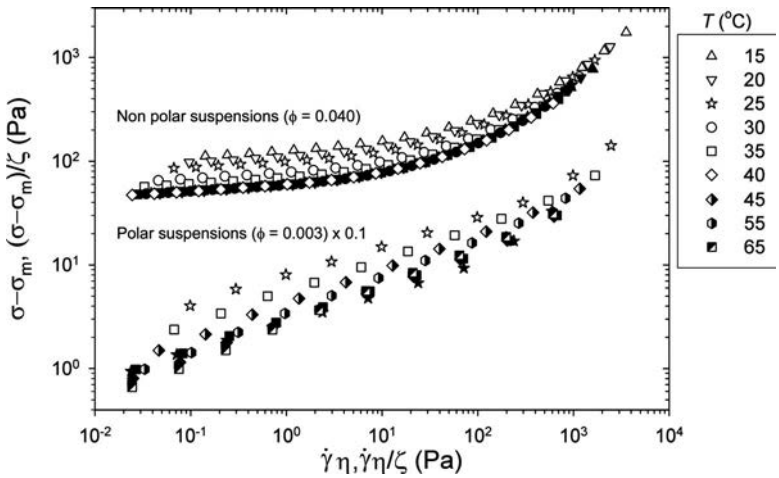

FIG. 8. Temperature dependency of σ-σ_m (unfilled and semi-filled symbols) and its scaling behavior (filled symbols) for the non-polar suspension prepared by ultrasonication (ϕ=0.04) and the polar suspension (ϕ =0.003); data for the polar suspension have been multiplied by 0.1.

stress measurements and the results are reported in Fig. 9. All the dynamic measurements were preceded by a pre-shearing followed by a 5400 rest time. For the non-polar suspension, two pre-shearing amplitudes were tested with initial hydrodynamic stresses, $\dot{\gamma}_i\eta$, equal to 0.95 and 95 Pa, while a pre-shearing at $\dot{\gamma}_i\eta < 0.1$ Pa with $\dot{\gamma}_i = 10^{-3}$ s^{-1} was used for the polar suspension. The variation of G' induced by the temperature dependency of the suspending fluid was taken into account by applying the time-temperature superposition. For that reason, the data were horizontally shifted with the respective factors a_T of the suspending fluids, relative to the reference temperature, T_{ref}, of 25 °C. The non-superposition of the plateau storage modulus, G'_0, at low frequencies shown in Fig. 9(a) for both suspensions reflects structure differences with temperature. However, in Fig. 9(b), data are shown to scale in single master curves using the shift factors a_T of the suspending fluids and κ. The shift factors κ for the non-polar suspensions following low ($\dot{\gamma}_i\eta = 0.95$ Pa) and high ($\dot{\gamma}_i\eta = 95$ Pa) pre-shearing stresses and for the polar suspensions ($\dot{\gamma}_i\eta = 0.1$ Pa) are reported in Fig. 10, along with the shift factors ξ used for the non-

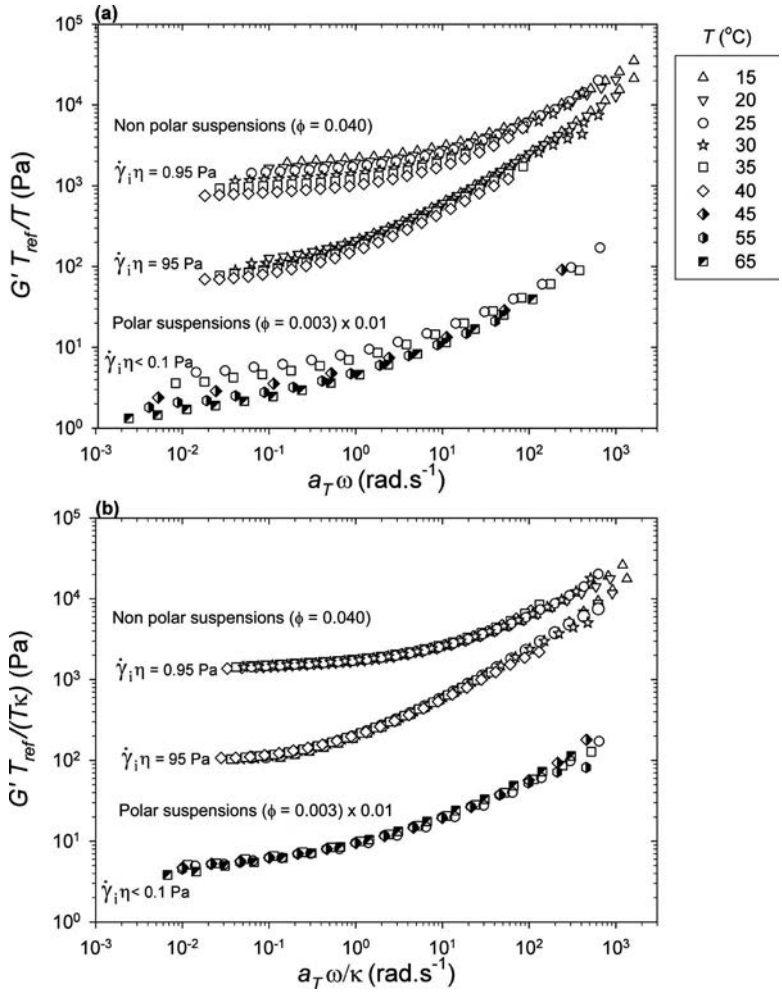

FIG. 9. (a) Temperature dependency of G' and (b) its scaling behavior for the non-polar suspension prepared by ultrasonication (ϕ=0.040) and the polar suspension (ϕ=0.003); data for the polar suspension have been multiplied by 0.1.

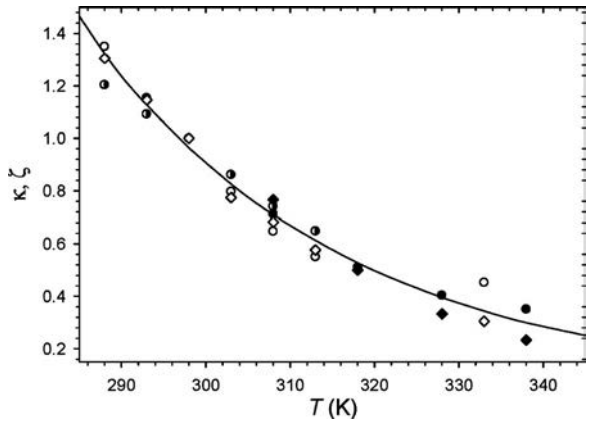

FIG. 10. Temperature dependency of the shift factors κ (circles) and ξ (diamonds) for the non-polar suspension prepared by ultrasonication (ϕ=0.040, unfilled symbols: $\dot{\gamma}_i\eta$=0.95 Pa; semi-filled symbols: $\dot{\gamma}_i\eta$=0.95 Pa) and for the polar suspension (filled symbols ϕ=0.003). Solid line represents the best fit using an exponential decay: $\kappa, \xi = 6673 \times e^{-0.03T}$.

equilibrium structures (used in Fig. 8). Both shift factors are shown to follow the same exponential decay dependency with temperature within measurement accuracy, but they are not equal for all conditions investigated. Nevertheless, the temperature dependencies of the polar and non-polar suspensions as well as the temperature dependencies of the equilibrium and non-equilibrium structures are similar.

D. Correlation between rheological properties and microstructure

The power-law dependencies of G_0' and of the apparent yield stress, σ_0, on the volume fraction depicted in Fig. 7(a) suggest that the microstructures of the polar and non-polar suspensions are fractal in nature. The scaling exponents n for G_0' and t for σ_0 of the two suspensions do not differ much within their determination accuracy (see Table I). Note that the two different pre-shearing conditions (low and high $\dot{\gamma}_i\eta$) lead to similar exponents n. The limit of linearity of γ^0 for the two suspensions is also shown to follow a power-law relationship with the volume fraction [Fig. 7(b)] with a negative exponent B (Table I). As mentioned earlier, the limit of linearity was established according to the variation of G' with strain. Above γ^0, while G' decreased continuously, G'' exhibited a maximum (results not shown). Similar behaviors were reported by Yziquel *et al.* (1999) for fumed silica suspensions and by Page *et al.* (2002) for coating colors. The maximum (overshoot) was observed to strongly decrease with increasing frequency and decreasing volume fraction. It allows classifying the nonlinear viscoelastic behavior of these suspen-

TABLE I. Values of the scaling exponents n, B, β, and t and fractal dimensions D_f of non-polar and polar suspensions.

Sample		n	B	D_f	β	t (D_f)[b]
Non-polar suspensions[a]	$\dot{\gamma}\eta$=0.95 Pa	2.2	−0.7	1.7	2.8	1.7 (1.8)
	$\dot{\gamma}\eta$=95 Pa	2.6				
Polar suspensions	$\dot{\gamma}\eta$<0.10 Pa	2.6	−0.6	2	2.6	2.3 (2.1)

[a]Non-polar suspensions prepared by ultrasonication.
[b]D_f derived from Eq. (7).

sions to type III or weak strain overshoot, according to Hyun *et al.* (2002). From the fractal scaling theory of Shih *et al.* (1990), a decrease of γ^0 with increasing volume fraction indicates that the elasticity of the system is ruled by the intra-microscopic elasticity K_{ξ_c}, which is lower than the inter-microscopic elasticity K_l. However, in the case of our suspensions, the volume fraction dependency of γ^0 is weak, which suggests mutual contributions of the two levels of elasticity. Actually, the theory of Shih *et al.* (1990), which only considers K_{ξ_c} in the strong-link regime, fails by predicting an unphysical negative value for the fractal dimension x of the clusters in the case of our suspensions. On the other hand, the scaling model of Wu and Morbidelli (2001) takes into account the two levels of elasticity with a parameter α ranging from 0 to 1 for the strong-link and the opposite weak-link regimes, respectively. The determined power-law exponents n and B lead for the two types of suspensions to $\alpha \gtrsim 0.4$ if a realistic value of the fractal dimension x is considered (in the range of 1–1.3 for a colloidal gel). Consequently, the two types of suspensions belong to the transition regime for which both levels of elasticity

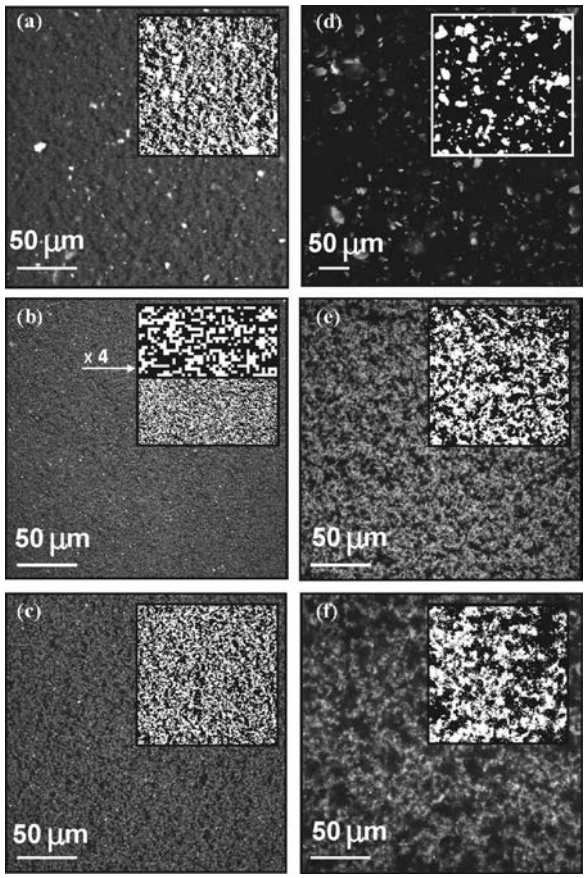

FIG. 11. CLSM images of the quiescent microstructures of the layered silicate suspensions. White areas are rich in layered silicate. Insets show the corresponding image part after binarization. The micrographs were taken at room temperature (about 23 °C). (a) 2.0% vol. of non-polar suspension (Cloisite 15A) prepared by ultrasonication; (b) 2.0% vol. of non-polar suspension (Cloisite 15A) prepared by solution mixing; (c) 1.0% vol. of non-polar suspension (Cloisite 15A) prepared by solution mixing; (d) 2.0% vol. of non-polar suspension of (Cloisite 30B) prepared by solution mixing; (e) 0.30% vol. of polar suspension (natural clay) prepared by solution mixing; (f) 0.15% vol. of polar suspension (natural clay) prepared by solution mixing.

contribute significantly to the overall elasticity. The values of the fractal dimensionalities D_f for the two types of suspensions derived from Eqs. (5) and (6) are close to 2 (see Table I). This supports the fact that their structures are similar. They are also in good agreement with the predictions only based on yield stress [Eq. (7) and Table I].

Real space observations of the microstructures of the non-polar and polar suspensions were done using CLSM. Figure 11 shows microstructural images from CLSM when no pre-shearing, except a slight squeezing flow to insert the sample within the CLSM holder gap, was imposed prior to their acquisition. The areas rich in fluorescent layered silicate appear bright in the micrographs. The dense regions in layered silicate within the non-polar suspensions prepared either by ultrasonication [Fig. 11(a), ϕ=0.020] or by solution mixing [Fig. 11(b), ϕ=0.020], and the polar suspension [Fig. 11(e), ϕ=0.003], form a continuous network with an overall appearance similar to those reported for polymer gels [Bremer *et al.* (1993); Crompton *et al.* (2005); Firoozmand *et al.* (2007); Hirokawa *et al.* (1999)]. The space-filling networks are consistent with the fractal structures inferred previously. At the micro-scale, these networks were shown to be static over the time scale of observation ($\sim$60 min), indicating the dominance of prevailing attraction forces over Brownian forces. It is also noteworthy to mention that the non-polar suspension based on the more polar organomodified montmorillonite (Cloisite 30B) did not exhibit such networks [Fig. 11(d)]. For a volume fraction of ϕ=0.020, the microstructure of the non-polar suspension prepared by ultrasonication [Fig. 11(a)] is shown to contain some large agglomerates in contrast to the suspension prepared by solution mixing [Fig. 11(b)]. The clay platelets contained within these agglomerates do not contribute to the percolation of the network, which explains the weaker rheological properties reported previously for this suspension (Figs. 5 and 6). By considering Eq. (5) with the low plateau value of the storage modulus G'_0 given in Fig. 5 (with $\dot{\gamma}_i = 10^{-3}$ s^{-1}) and assuming the same fractal dimensionality D_f and similar β (Table I) for both suspensions, the network induced by ultrasonication is expected to include only approximately one half of the total clay volume fraction. Consequently, and due to its fractal nature, it should have a characteristic length scale, ξ_0, larger than that of the network prepared by solution mixing (Eq. (1), assuming ξ_0 is proportional to ξ_c [Gefen *et al.* (1981)]). Its coarser microstructure observed by CLSM [Fig. 11(a) vs. Fig. 11(b)] qualitatively confirmed this trend, but this should be considered with care since the two preparation methods involve different flow histories. In the next paragraph, the microstructure characteristic size ξ_0 is actually observed to depend on the pre-shearing rate. Similarly, a more open network is seen when the volume fraction of the non-polar suspension is decreased by half to 0.010 [Fig. 11(c) compared to Fig. 11(b)]. In contrast, the polar suspension exhibits the same behavior when the volume fraction is decreased from 0.003 [Fig. 11(e)] to 0.0015 [Fig. 11(f)]. Figure 12 presents the distance distribution function, $P(\xi)$, used to quantify the network characteristic length scale ξ_0 of the CLSM images of Fig. 11. The observable isotropy of the quiescent microstructures is confirmed by the similarity of the ξ distributions along the x and y directions. The corresponding characteristic length scales, ξ_0 [shown in the legends of Figs. 12(a) and 12(b)], are in agreement with the main concept of fractal scaling theories described by Eq. (1). Actually, according to this equation and the mass-fractal dimensionalities, D_f, given in Table I, an increase by a factor of 2 of the volume fraction would result in a decrease of ξ_0 by factors of 0.5 and 0.6 for the polar and non-polar suspensions prepared by solution mixing, respectively. These theoretical values are in close agreement with their corresponding experimental factors equal to 0.5 ± 0.05 for the two suspensions. In addition, the order of magnitude of the characteristic length scales, ξ_0, of the non-polar and polar suspensions are similar while the volume fraction range for the polar suspensions is one decade smaller. The differences in the range of

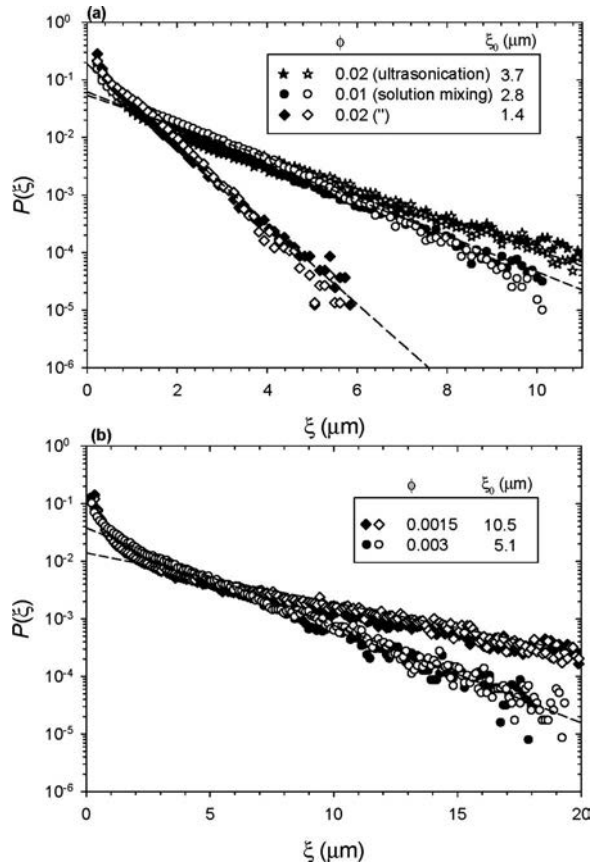

FIG. 12. ξ distributions along x (unfilled symbols) and y (filled symbols) directions for the (a) non-polar suspensions and (b) polar suspensions. Dashed lines represent log-linear regressions.

volume fractions result in different sizes a_{eff} of the compact building blocks of the clusters, as calculated from Eq. (1). This equation predicts that the compact building blocks of the non-polar suspensions are almost three times larger than those of the polar suspensions [ratio of Eq. (1)for the non-polar and polar suspensions estimated from ξ_0 of Fig. 12 and the fractal dimensions from Table I]. This is attributed to differences in the nanoscale interactions between the particles during the solution mixing step in preparing the suspensions. Actually, it has been shown that the organomodified clay in toluene forms tactoids of 3–6 platelets whereas the natural clay is fully exfoliated in de-ionized water [Ho *et al.* (2001,2002); Ho and Glinka (2003)]. Finally, the comparable rheological properties of these suspensions observed on different volume fraction ranges are explained by differences in the elastic constant K. From Eq. (5) and using the scaling exponents and fractal dimensions given in Table I, one obtains the elastic constant K for the polar suspensions nearly 100 times larger than for the non-polar suspensions. Assuming that the elasticity is governed by the interaction potential between particles and clusters [Pantina and Furst (2006)], the interaction potential level within the polar suspensions is therefore much higher than that within the non-polar ones.

Figure 13 reports micrographs for the metastable microstructures of the non-polar suspension prepared by solution mixing (ϕ=0.020) and polar suspension (ϕ=0.003) following various pre-shearing rates $\dot{\gamma}_i$ from 10 to 10^{-2} s^{-1}. Their elasticity is given by

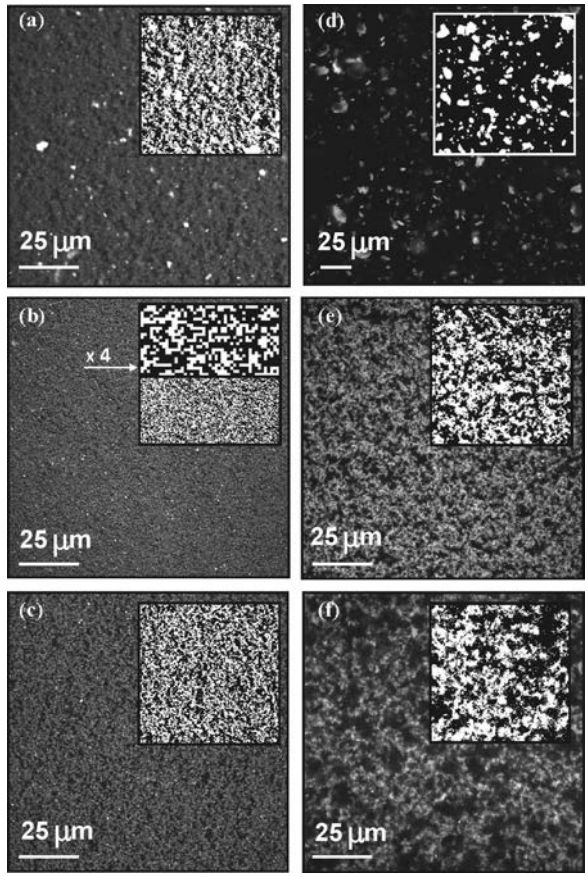

FIG. 13. Effect of the pre-shearing amplitude on the flow-induced metastable microstructures of the layered silicate suspensions. Right: 2 vol. % non-polar and left: 0.3 vol. % polar suspensions prepared by solution mixing (a) pre-shear rate of 10, (b) 1, (c) 0.1, and (d) 0.01 s^{-1}. The pre-shearing flow direction was from bottom to top. Insets show the corresponding image parts after binarization. The micrographs were taken at room temperature (about 23 °C).

G'_∞ in Fig. 2. These metastable microstructures reflect their corresponding non-equilibrium microstructures, since no overall structural recovery at the micro-scale was observed in CLSM upon cessation of steady shear flow. Therefore, the structure build-up at rest resulting in the increase of G' from G'_i to G'_∞ depicted in Fig. 1 is due to local rearrangements at smaller length scales. The lack of micro-structural recovery toward a single equilibrium structure outlines the high interparticle attraction energy ($>20\ k_BT$), a characteristic of strongly aggregated systems. On the shear rate range investigated, from 10^{-2} to 10 s^{-1}, the metastable microstructures of the polar suspensions display no apparent anisotropy, while for the non-polar suspensions a slight one along the vorticity direction is distinguishable, with the difference in the ξ distributions along the x and y directions (Fig. 12). A constant surface coverage by the structure was also observed on the shear rate range explored, with A (described in the optical measurement section) equal to 0.48 ± 0.02 and 0.39 ± 0.02 for the non-polar and polar suspensions, respectively. The metastable structures and, hence, the non-equilibrium structures differ essentially from each other by their characteristic length scale, ξ_0, which tends to decrease for increasing pre-shearing rate amplitude $\dot{\gamma}_i$ as revealed quantitatively in Fig. 14. A comparable aggre-

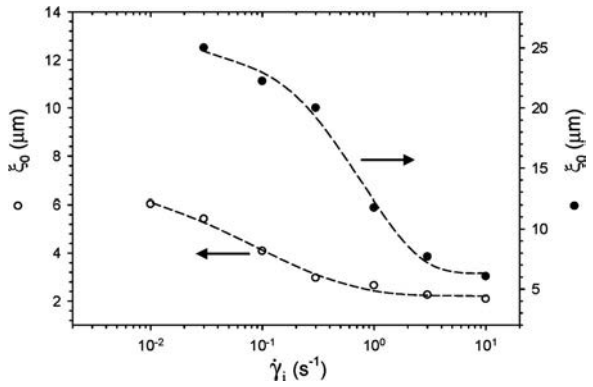

FIG. 14. Dependence of the characteristic length scale ξ_0 with the pre-shearing amplitude $\dot{\gamma}_i$ for the non-polar (unfilled symbols) and polar suspension (filled symbols) metastable structures.

gation process was recently reported by Rahatekar *et al.* (2006) for a carbon nanotube suspension in epoxy. The dependency of the rheological properties with the pre-shearing and shearing amplitudes (Figs. 2, 3, and 8) results consequently from the shear-controlled characteristic length scale of the microstructure, as supported by the strong correlation between G'_∞ (Fig. 2) and ξ_0 (Fig. 14). This structural dependency is attributed to a reversible shear-induced aggregation. As a result, ξ_0 follows a power-law dependency at intermediate shear rates with a power exponent $m=-0.22$ for the non-polar suspensions and $m=-0.42$ for the polar suspensions. Sonntag and Russel (1986, 1987) reported a value of $m=-0.35$ for their dilute flocculated suspensions (polystyrene lattices). These values are within the limits of -0.23 and -0.5 determined by Potanin (1993) using computer simulations. The low limit is related to the non-central components of the particle attraction potential (function of the angle between adjacent bonds), while the high limit belongs to the purely central component (function of the distance between the centers of neighboring particles).

Finally, the shear-induced aggregation has been directly visualized during stepwise reductions in shear rate from 10 to 10^{-2} s^{-1}. Figure 15 reports the resulting transient stress response, σ^-, and characteristic length scale, ξ_0, as a function of strain for the polar

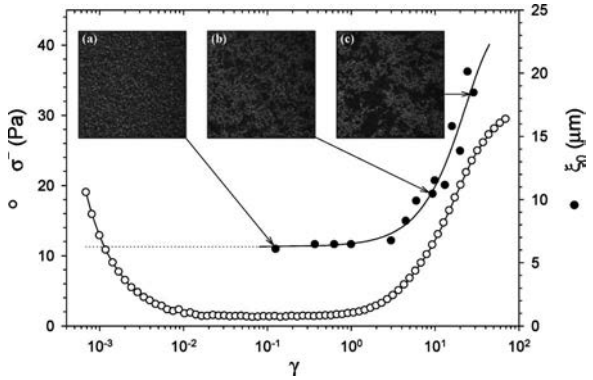

FIG. 15. σ (unfilled symbols) and ξ_0 (filled symbols) as functions of γ after a stepwise reduction in the shear rate from 10 to 10^{-2} s^{-1} for the polar suspension (ϕ=0.003). Insets show CLSM images at different deformation values: (a) 0.13, (b) 10, and (c) 29. Solid line is drawn to guide the eyes.

suspension (ϕ=0.003). The first decrease in σ^- at short times, corresponding to the viscoelastic response of the suspension (stress relaxation), is followed by a monotonic increase as ξ_0 starts to increase due to the shear-induced aggregation. The transient stress response at large deformations is therefore shown to be governed by a structural evolution at the micro-scale. Similar observations have been made for the non-polar suspensions.

V. CONCLUDING REMARKS

In this paper, the nature of flow-induced non-equilibrium and metastable structures of polar and non-polar nanoclay suspensions has been probed by studying the scaling behavior of their linear and non-linear viscoelastic properties and by quantifying real space observations obtained with CLSM. The power-law dependencies of the viscoelastic properties with the volume fraction have been interpreted in light of the fractal nature of the suspensions. Fractal dimensions close to 2 were estimated using the scaling model of Wu and Morbidelli (2001). Direct observations of the microstructures using CLSM confirmed the presence of fractal networks with fractal dimensions $\sim$2 for both types of suspensions. As far as we are aware, such CLSM observations for colloidal suspensions under shear flow have never been reported. They demonstrate the potential of CLSM to correlate the complex rheological behavior of colloidal suspensions with their underlying structures.

The similar rheological properties of the non-polar and polar suspensions were explained to arise from differences in particle interaction potential, while the volume fraction for the polar suspension was ten times smaller. The attraction potential responsible for the fractal networks was clarified owing to its temperature dependency. The exponential decay of the shift factors with temperature was shown to be similar for the two suspensions.

By increasing the shearing amplitude, the characteristic length scale of the non-equilibrium microstructures was shown to decrease from high to low plateau values. This structural variation with the shearing amplitude was attributed to a reversible shear-induced aggregation. Upon cessation of flow, no overall structural recovery at the micro-scale was observed in CLSM, leading to metastable microstructures with the same characteristic length scale than their non-equilibrium counterparts. Consequently, the thixotropic behavior of these suspensions is due to local rearrangements at the nano-scale and its physical interpretation should be elucidated using wide-angle scattering techniques. Based on these findings, the rheological dependency on the flow history is attributed to the shear-controlled characteristic length scale of the microstructure.

ACKNOWLEDGMENTS

The authors are most grateful to Dr. N. Tran-Khanh and Dr. M. Thibault for their precious help with CLSM experiments. They also thank Professor M. Bousmina for the use of the Linkham shear cell. One of the authors (C.M.) is thankful to Alcan Inc. for a scholarship. Southern Clay Products kindly provided the nanoclays used in this study. Finally, financial support from NSERC (Natural Science and Engineering Research Council of Canada) and from FQRNT (Fonds Québécois de Recherche en Nature et Technologies) is gratefully acknowledged.

References

Aubry, T., T. Razafinimaro, and P. Mederic, "Rheological investigation of the melt state elastic and yield properties of a polyamide-12 layered silicate nanocomposite," J. Rheol. **49**, 425–440 (2005).

Bousmina, M., "Study of intercalation and exfoliation processes in polymer nanocomposites," Macromolecules **39**, 4259–4263 (2006).

Bremer, L. G. B., B. H. Bijsterbosch, P. Walstra, and T. Vanvliet, "Formation, properties and fractal structure of particle gels," Adv. Colloid Interface Sci. **46**, 117–128 (1993).

Bremer, L. G. B., T. Vanvliet, and P. Walstra, "Theoretical and experimental-study of the fractal nature of the structure of casein gels," J. Chem. Soc., Faraday Trans. 1 **85**, 3359–3372 (1989).

Buscall, R., P. D. A. Mills, J. W. Goodwin, and D. W. Lawson, "Scaling behaviour of the rheology of aggregate networks formed from colloidal particles," J. Chem. Soc., Faraday Trans. **84**, 4249–4260 (1988).

Bushell, G. C., Y. D. Yan, D. Woodfield, J. Raper, and R. Amal, "On techniques for the measurement of the mass fractal dimension of aggregates," Adv. Colloid Interface Sci. **95**, 1–50 (2002).

Cadene, A., S. Durand-Vidal, P. Turq, and J. Brendle, "Study of individual Na-montmorillonite particles size, morphology, and apparent charge," J. Colloid Interface Sci. **285**, 719–730 (2005).

Crassous, J. J., R. Regisser, M. Ballauff, and N. Willenbacher, "Characterization of the viscoelastic behavior of complex fluids using the piezoelastic axial vibrator," J. Rheol. **49**, 851–863 (2005).

Crompton, K. E., R. J. Prankerd, D. M. Paganin, T. F. Scott, M. K. Horne, D. I. Finkelstein, K. A. Gross, and J. S. Forsythe, "Morphology and gelation of thermosensitive chitosan hydrogels," Biophys. Chem. **117**, 47–53 (2005).

Dullaert, K., and J. Mewis, "Stress jumps on weakly flocculated dispersions: Steady state and transient results," J. Colloid Interface Sci. **287**, 542–551 (2005).

Durmus, A., A. Kasgoz, and C. W. Macosko, "Linear low density polyethylene (LLDPE)/clay nanocomposites. Part I: Structural characterization and quantifying clay dispersion by melt rheology," Polymer **48**, 4492–4502 (2007).

Firoozmand, H., B. S. Murray, and E. Dickinson, "Fractal-type particle gel formed from gelatin+starch solution," Langmuir **23**, 4646–4650 (2007).

Galgali, G., C. Ramesh, and A. Lele, "Rheological study on the kinetics of hybrid formation in polypropylene nanocomposites," Macromolecules **34**, 852–858 (2001).

Gefen, Y., A. Aharony, B. B. Mandelbrot, and S. Kirkpatrick, "Solvable fractal family, and its possible relation to the backbone at percolation," Phys. Rev. Lett. **47**, 1771–1774 (1981).

Götze, W., *Aspects of Structural Glass Transitions* (Elsevier, Les Houches, 1991).

Helgeson, M. E., N. J. Wagner, and D. Vlassopoulos, "Viscoelasticity and shear melting of colloidal star polymer glasses," J. Rheol. **51**, 297–316 (2007).

Hirokawa, Y., H. Jinnai, Y. Nishikawa, T. Okamoto, and T. Hashimoto, "Direct observation of internal structures in poly(N-isopropylacrylamide) chemical gels," Macromolecules **32**, 7093–7099 (1999).

Ho, D. L., and C. J. Glinka, "Effects of solvent solubility parameters on organoclay dispersions," Chem. Mater. **15**, 1309–1312 (2003).

Ho, D. L., R. M. Briber, and C. J. Glinka, "Characterization of organically modified clays using scattering and microscopy techniques," Chem. Mater. **13**, 1923–1931 (2001).

Ho, D. L., R. M. Briber, and C. J. Glinka, *Studies of Organically Modified Clays by Scattering Techniques* (Oxford University Press, San Francisco, 2002).

Hobbie, E. K., and D. J. Fry, "Rheology of concentrated carbon nanotube suspensions," J. Chem. Phys. **126**, 124907 (2007).

Hyun, K., S. H. Kim, K. H. Ahn, and S. J. Lee, "Large amplitude oscillatory shear as a way to classify the complex fluids," J. Non-Newtonian Fluid Mech. **107**, 51–65 (2002).

Jogun, S., and C. F. Zukoski, "Rheology of dense suspensions of platelike particles," J. Rheol. **40**, 1211–1232 (1996).

Jogun, S. M., and C. F. Zukoski, "Rheology and microstructure of dense suspensions of plate-shaped colloidal particles," J. Rheol. **43**, 847–871 (1999).

Kantor, Y., and I. Webman, "Elastic properties of random percolating systems," Phys. Rev. Lett. **52**, 1891–1894

(1984).

Kaufman, L. J., C. P. Brangwynne, K. E. Kasza, E. Filippidi, V. D. Gordon, T. S. Deisboeck, and D. A. Weitz, "Glioma expansion in collagen I matrices: Analyzing collagen concentration-dependent growth and motility patterns," Biophys. J. **89**, 635–650 (2005).

Khan, S. A. and N. J. Zoeller, "Dynamic rheological behavior of flocculated fumed silica suspensions," J. Rheol. **37**, 1225–1235 (1993).

King, H. E., S. T. Milner, M. Y. Lin, J. P. Singh, and T. G. Mason, "Structure and rheology of organoclay suspensions," Phys. Rev. E **75**, 021403 (2007).

Krall, A. H., and D. A. Weitz, "Internal dynamics and elasticity of fractal colloidal gels," Phys. Rev. Lett. **80**, 778–781 (1998).

Kroon, M., W. L. Vos, and G. H. Wegdam, "Structure and formation of a gel of colloidal disks," Phys. Rev. E **57**, 1962–1970 (1998).

Lim, Y. T., and O. O. Park, "Phase morphology and rheological behavior of polymer/layered silicate nanocomposites," Rheol. Acta **40**, 220–229 (2001).

Lin, Y. C., G. H. Koenderink, F. C. MacKintosh, and D. A. Weitz, "Viscoelastic properties of microtubule networks," Macromolecules **40**, 7714–7720 (2007).

Lyatskaya, Y., and A. C. Balazs, "Modeling the phase behavior of polymer-clay composites," Macromolecules **31**, 6676–6680 (1998).

Mason, T. G. and D. A. Weitz, "Linear viscoelasticity of colloidal hard sphere suspensions near the glass transition," Phys. Rev. Lett. **75**, 2770–2773 (1995).

Mellema, M., J. W. M. Heesakkers, J. H. J. van Opheusden, and T. van Vliet, "Structure and scaling behavior of aging rennet-induced casein gels examined by confocal microscopy and permeametry," Langmuir **16**, 6847–6854 (2000).

Michot, L. J., I. Bihannic, K. Porsch, S. Maddi, C. Baravian, J. Mougel, and P. Levitz, "Phase diagrams of Wyoming Na-montmorillonite clay. Influence of particle anisotropy," Langmuir **20**, 10829–10837 (2004).

Mitchell, C. A., and R. Krishnamoorti, "Rheological properties of diblock copolymer/layered-silicate nanocomposites," J. Polym. Sci. **40**, 1434–1443 (2002).

Mobuchon, C., P. Carreau, and M.-C. Heuzey, "Effect of flow history on the structure of a non-polar polymer/clay nanocomposite model system," Rheol. Acta **46**, 1045–1056 (2007).

Mourchid, A., A. Delville, J. Lambard, E. Lecolier, and P. Levitz, "Phase-diagram of colloidal dispersions of anisotropic charged-particles—equilibrium properties, structure, and rheology of laponite suspensions," Langmuir **11**, 1942–1950 (1995).

Page, A., P. J. Carreau, M. Moan, and M. C. Heuzey, "Rheological behavior of coating colors: Influence of thickener," Can. J. Chem. Eng. **80**, 1181–1188 (2002).

Pantina, J. P., and E. M. Furst, "Colloidal aggregate micromechanics in the presence of divalent ions," Langmuir **22**, 5282–5288 (2006).

Patel, H. A., R. S. Somani, H. C. Bajaj, and R. V. Jasra, "Nanoclays for polymer nanocomposites, paints, inks, greases and cosmetics formulations, drug delivery vehicle and waste water treatment," Bull. Mater. Sci. **29**, 133–145 (2006).

Pawley, J. B., *Handbook of Biological Confocal Microscopy* (Springer, Madison, 2006).

Piau, J. M., M. Dorget, and J. F. Palierne, "Shear elasticity and yield stress of silica-silicone physical gels: Fractal approach," J. Rheol. **43**, 305–314 (1999).

Pignon, F., A. Magnin, and J.-M. Piau, "Thixotropic colloidal suspensions and flow curves with minimum: Identification of flow regimes and rheometric consequences," J. Rheol. **40**, 573–587 (1996).

Pignon, F., A. Magnin, and J. M. Piau, "Butterfly light scattering pattern and rheology of a sheared thixotropic clay gel," Phys. Rev. Lett. **79**, 4689–4692 (1997b).

Pignon, F., A. Magnin, and J.-M. Piau, "Thixotropic behavior of clay dispersions: Combinations of scattering and rheometric techniques," J. Rheol. **42**, 1349–1373 (1998).

Pignon, F., A. Magnin, J.-M. Piau, B. Cabane, P. Lindner, and O. Diat, "Yield stress thixotropic clay suspension: investigations of structure by light, neutron, and x-ray scattering," Phys. Rev. E **56**, 3281–3289 (1997a).

Potanin, A. A., "On the computer simulation of the deformation and breakup of colloidal aggregates in shear flow," J. Colloid Interface Sci. **157**, 399–410 (1993).

Rahatekar, S. S., K. K. K. Koziol, S. A. Butler, J. A. Elliott, M. S. P. Shaffer, M. R. Mackley, and A. H. Windle, "Optical microstructure and viscosity enhancement for an epoxy resin matrix containing multiwall carbon nanotubes," J. Rheol. **50**, 599–610 (2006).

Ren, J., A. S. Silva, and R. Krishnamoorti, "Linear viscoelasticity of disordered polystyrene-polyisoprene block copolymer based layered-silicate nanocomposites," Macromolecules **33**, 3739–3746 (2000).

Ruzicka, B., L. Zulian, and G. Ruocco, "More on the phase diagram of laponite," Langmuir **22**, 1106–1111 (2006).

Saint-Michel, F., F. Pignon, and A. Magnin, "Fractal behavior and scaling law of hydrophobic silica in polyol," J. Colloid Interface Sci. **267**, 314–319 (2003).

Segrè, P. N., V. Prasad, A. B. Schofield, and D. A. Weitz, "Glasslike kinetic arrest at the colloidal-gelation transition," Phys. Rev. Lett. **86**, 6042–6045 (2001).

Shalkevich, A., A. Stradner, S. K. Bhat, F. Muller, and P. Schurtenberger, "Cluster, glass, and gel formation and viscoelastic phase separation in aqueous clay suspensions," Langmuir **23**, 3570–3580 (2007).

Shih, W.-H., W. Y. Shih, S.-I. Kim, J. Liu, and I. A. Aksay, "Scaling behavior of the elastic properties of colloidal gels," Phys. Rev. A **42**, 4772–4779 (1990).

Sonntag, R. C., and W. B. Russel, "Structure and breakup of flocs subjected to fluid stresses: I. Shear experiments," J. Colloid Interface Sci. **113**, 399–413 (1986).

Sonntag, R. C., and W. B. Russel, "Structure and breakup of flocs subjected to fluid stresses: II. Theory," J. Colloid Interface Sci. **115**, 378–389 (1987).

Tanaka, H., S. Jabbari-Farouji, J. Meunier, and D. Bonn, "Kinetics of ergodic-to-nonergodic transitions in charged colloidal suspensions: Aging and gelation," Phys. Rev. E **71**, 021402 (2005).

Tanaka, H., J. Meunier, and D. Bonn, "Nonergodic states of charged colloidal suspensions: Repulsive and attractive glasses and gels," Phys. Rev. E **69**, 031404 (2004).

Thompson, D. W., and J. T. Butterworth, "The nature of laponite and its aqueous dispersions," J. Colloid Interface Sci. **151**, 236–243 (1992).

Tombacz, E., and M. Szekeres, "Colloidal behavior of aqueous montmorillonite suspensions: the specific role of *p*H in the presence of indifferent electrolytes," Appl. Clay Sci. **27**, 75–94 (2004).

Trappe, V., V. Prasad, L. Cipelletti, P. N. Segre, and D. A. Weitz, "Jamming phase diagram for attractive particles," Nature (London) **411**, 772–775 (2001).

Trappe, V., and D. A. Weitz, "Scaling of the viscoelasticity of weakly attractive particles," Phys. Rev. Lett. **85**, 449–452 (2000).

Trappe, V., and P. Sandkuhler, "Colloidal gels–low-density disordered solid-like states," Curr. Opin. Colloid Interface Sci. **8**, 494–500 (2004).

Vermant, J., S. Ceccia, M. K. Dolgovskij, P. L. Maffettone, and C. W. Macosko, "Quantifying dispersion of layered nanocomposites via melt rheology," J. Rheol. **51**, 429–450 (2007).

Wu, H., and M. Morbidelli, "Model relating structure of colloidal gels to their elastic properties," Langmuir **17**, 1030–1036 (2001).

Yziquel, F., P. J. Carreau, and P. A. Tanguy, "Non-linear viscoelastic behavior of fumed silica suspensions," Rheol. Acta **38**, 14–25 (1999).

Zaccarelli, E., G. Foffi, K. A. Dawson, F. Sciortino, and P. Tartaglia, "Mechanical properties of a model of attractive colloidal solutions," Phys. Rev. E **63**, 031501 (2001).